

Impact of top-surface morphology on CO₂ storage capacity[☆]

Halvor Møll Nilsen^a, Anne Randi Syversveen^b, Knut-Andreas Lie^{a,d}, Jan Tveranger^c, Jan M. Nordbotten^d

^a*SINTEF ICT, PO Box 124, Blindern, N-0314 Oslo, Norway*

^b*Norwegian Computing Center, PO Box 114, Blindern, N-0314 Oslo, Norway*

^c*Center for Integrated Petroleum Research, Uni Research, PO Box 7800, N-5020 Bergen, Norway*

^d*Department of Mathematics, University of Bergen, PO Box 7800, N-5020 Bergen, Norway*

Abstract

Long-term forecasting of the behaviour of CO₂ injected in industrial quantities into sub-surface reservoirs is generally performed using models including very limited geological detail. This practise, although dictated by restrictions with respect to model resolution and CPU cost, partly rests on an unverified but widely held assumption that geological detail will not influence simulation outcomes on the spatial and temporal scales relevant for geological sequestration. The present study aims to partly assess the validity of this assumption by selecting a series of realistic geological features and investigate their impact when modelling CO₂ sequestration.

Injected CO₂ is primarily retained in structural and stratigraphic traps at the top of the reservoir interval. We will therefore investigate how different top-surface morphologies will influence the CO₂ storage capacity. To this end, a series of different top surfaces are created by combining different stratigraphic scenarios with different structural scenarios. The models are created stochastically to quantify uncertainty. Theoretical upper bounds on the volume available for structural trapping are established by a geometrical analysis. Estimates for actual trapping from a single point source are calculated in a simplified and efficient manner by a spill-point analysis and more

[☆]The full data sets and additional illustrations are available from the IGEMS webpage: <http://igems.nr.no/>

accurately by a detailed flow simulation that assumes vertical equilibrium. Results from the two approaches are compared. For the fluid flow simulation method, we investigate the effect of grid resolution. The experiments show that the morphology of the top seal is of great importance for the storage capacity and migration patterns and that the effect of upscaling is highly structure dependent.

Keywords: structural trapping, spill point analysis, upscaling, uncertainty analysis

1. Introduction

To reduce carbon emissions to the atmosphere, storing CO₂ in deep sub-surface rock formations has become an important issue. Most of the technology required to inject and store CO₂ in saline aquifers, unminable coal seams, or abandoned petroleum reservoirs is already available from the petroleum and mining industry. The main question is the cost and risk associated with the storage operation. Three elements are essential to consider CO₂ storage in a specific location. First, there must be sufficient pore volume to store all the CO₂. Second, there must be an intact top-seal to ensure containment, and, finally, injection should be possible within operational constraints.

A significant number of research projects involving field testing of sub-surface CO₂ storage exist worldwide (see www.ieaghg.org). The main purpose of most of these studies is to investigate practical and technical challenges related to sequestering CO₂ in underground formations. None of these practical tests involve volumes, rates, and time scales approaching the envisaged requirements for long-term geological storage of gigatonnes of CO₂. Assessments of feasibility and safety of long-term storage of significant volumes of CO₂ at a particular site must be based on reliable, model-based forecasting of sub-surface behaviour of CO₂. Models employed for this purpose should ideally include all parameters likely to affect the outcome. Nevertheless, in this context many geological parameters are overlooked, ignored or considered to have insignificant impact at temporal and spatial scales relevant to geological storage of CO₂. There is an obvious need to address the handling and implementation of geological parameters and their impact on CO₂ sequestration in a methodical manner. This will in turn give constraints with respect to which parameters should be included in large-scale, long-term simulation of CO₂ sequestration.

Site characterisation for sequestration purposes on an industrial scale largely centres on establishing storage capacity, injectivity potential, CO₂ interaction with the surrounding rocks and fluids, and assessing containment and potentially detrimental impact on natural resources. To this end, comprehensive numerical simulation capabilities have been developed (Celia et al., 2010; Class et al., 2009), but academic studies and community benchmarks of CO₂ injection have so far largely focused on numerical and modelling-based uncertainties (Pruess et al., 2004; Class et al., 2009), employing conceptual or highly simplified representations of subsurface geology and giving little attention to uncertainties originating from formation properties. In particular, we are missing systematic studies that investigate and develop a generic quantitative understanding of how formation properties and geometries impact large-scale CO₂ sequestration. Such studies would, in turn, allow qualified simplification of models by offering an “impact-ranking” of parameters and focus data collection for modelling purposes towards prioritising collection of data related to high-impact geological parameters.

Herein, we make a first step in this direction by considering a synthetic storage scenario in which the reservoir consists of good quality sand buried underneath an impermeable caprock that dips slightly in one direction. Supercritical CO₂ is a buoyant fluid, and after injection, it moves upwards, until encountering a barrier that prevents further movement. Then the fluid moves laterally upslope along the barrier until the end of the barrier or a trap is reached, where accumulation can take place. In particular, this means that the morphology of the top seal will affect CO₂ migration pathways, shape and size of traps, and the seal integrity on reservoir scale. In the following, we assume that top-surface morphology is the main driver of uncertainty. Using a simple model setup with virtually uniform properties but variable top-surface topography, we study how different reliefs in this morphology impact estimates of storage capacity and migration patterns. To this end, multiple geostatistical realisations of each sedimentological scenario are required to quantify the relative uncertainty associated with depositional and structural architecture and their associated petrophysical properties.

In the following, we outline the selection of the geological features chosen in our study, describe the overall design of our model set-up for studying their impact on CO₂ sequestration, briefly discuss generation of geostatistical realisations, present simulation results, and discuss the effects of upscaling to determine how much the models can be upscaled without losing important details

2. Selection of geological features

Geological storage of CO₂ benefits from experiences gained and tools developed by the petroleum industry over many decades, in particular with respect to subsurface data acquisition and handling, the use of reservoir modelling tools and methods for discretizing and quantifying geological features and properties from wells, seismic data and outcrop analogues. Fluid-flow simulation of hydrocarbon reservoirs also routinely involves assessing the interplay between geology and reservoir behaviour. However, despite obvious similarities with respect to the common need for a comprehensive understanding of formation properties, subsurface characterisation for large-scale CO₂ sequestration needs to consider a number of aspects normally not viewed as important in petroleum production models. The life-span of a producing petroleum reservoir is a few decades at most, focusing modelling towards considering reservoir dynamics and processes operating on a relatively short time scale. Regulations for CO₂ sequestration, on the other hand, stipulate forecasting on a scale of thousands of years, which implies taking into account a number of slow-acting processes such as tectonic movements, glaciations, sea level changes, and slow chemical reactions between the injected CO₂, pore-fluids, and rock. A further contrast is presented by spatial scale. Most hydrocarbon fields cover less than few tens square kilometres, whereas some planned CO₂ injection schemes envisage sequestration in formations covering several thousand square kilometres. To cut CPU cost, these contrasts in temporal and spatial scale are often taken as an argument in favour of employing simplified geological models when simulating long-term, large-scale CO₂ injection. However, the underlying assumption, that geological features proven important in hydrocarbon production may have a negligible impact on the scales employed for CO₂ sequestration, remains largely unsubstantiated as relevant studies are lacking.

The basic concept of the present study is broadly based on the approach taken by the SAIGUP project (Manzocchi et al., 2008), which ventured to assess the influence of geological factors on production by analysing a large suite of synthetic models generated by combining sedimentological models ranging from comparatively simple to highly complex with a series of structural scenarios. Our original intention to re-run parts of the SAIGUP model matrix, replacing petroleum production with CO₂ injection, had to be abandoned as the size of the SAIGUP model template (3.0 km × 9.0 km × 80 m) turned out to be too small, causing the injected CO₂ to migrate out of

the model area within a few years of simulation time, e.g., as discussed by Ashraf et al. (2010). Consequently a new model template had to be generated for the purpose of this study. It covers an area of 30 by 60 km and includes a 100 m thick reservoir unit. The overall shape is slightly convex and tilted one degree along its long-axis in order to control plume movement during simulation. The top of the reservoir is envisaged as capped by thick, impermeable shale and thus not explicitly included in our models.

To limit the scope of the present study, we decided to focus on a set of geological features in siliciclastic rocks that straddle seismic resolution in terms of scale and with a proven but as yet not systematically studied impact on CO₂ sequestration. Top reservoir topography fulfils this criterion as it has been observed to have a significant impact on CO₂ migration on 4D seismic data (Chadwick and Noy, 2010; Chadwick et al., 2010; Eiken et al., 2011), whereas its potential impact on sub-seismic scale has not been studied.

Geological features affecting the topography of the reservoir/seal interface are commonly only included in reservoir models if they have been explicitly mapped on seismic surveys. In general this implies that features with relief amplitudes below seismic resolution (i.e., about 10–15 m) are not captured explicitly in reservoir models (although sub-seismic faults may occasionally be included). Thus top reservoir topography, as seen in most reservoir models, is largely defined by tectonic features such as faults exceeding 10–15 m of displacement, and large-scale folding and tilting. This simplifies or overlooks the fact that top reservoir topography at or below seismic resolution can be affected by a number of factors such as draped or in-filled depositional or erosional relief, sub-seismic scale faults, laterally non-uniform compaction, various forms of diapirism and breccia pipes.

3. Geological features

We selected a series of depositional, erosional and tectonic features according to a set of criteria governed by our chosen horizontal model resolution of 100m × 100m and the overall requirement of providing “realistic” scenarios. Our choice of model resolution was influenced by the need to keep computational cost of the simulations within practical limits.

To match the scale and resolution of our model, we focus on geological features with reasonably predictable properties in terms of scales, geometries and distribution patterns and with a potential to produce recurrent and predictable spatial patterns in an area of 30 km by 60 km. Although features

such as diapirs, sand dykes, and breccia pipes can substantially influence top-reservoir configurations and integrity, their seismic and sub-seismic characteristics in terms of size, and spatial distribution on scales similar to our model area is poorly constrained by empirical data sets. The resulting lack of control of realistic model input parameters poses a problem when evaluating the generic influence of such features on fluid simulation outcomes.

A final requirement defined by the project was the “stratigraphic realism” of the features to be included in the model: Stratigraphic successions involving thick, impermeable shale sealing an underlying sandy reservoir unit, (forming our basic model set-up), are commonly products of substantial sea-level rise forcing a regional shift from sand to shale deposition. The chosen geological features influencing top reservoir topography should therefore be structures known to or expected to occur at such stratigraphic positions.

The chosen sedimentological features include: 1) buried beach ridges in a flooded marginal marine setting (FMM), and 2) buried offshore sand ridges (OSS). Both fulfil the above stated criteria by being resolvable features on the chosen modelling scale, straddling seismic resolution, having geometries and spatial distributions constrained by empirical data, and occur or may occur at the interface between a sandy reservoir unit and an overlying thick impermeable shale unit.

Buried beach ridges in a flooded marginal-marine setting (FMM). Beach ridges are defined as relict, semiparallel, multiple ridges, either wave (berm ridge) or wind (multiple backshore foredune) origin and usually forming strandplains Otvos (2000). They originate in the inter- and supratidal zone and may consist of either siliciclastic or calcareous material ranging from fine sand to cobbles and boulders. Strandplains with systems of more or less evenly spaced beach ridges commonly reflect forced shoreline progradation or falling relative sea level (e.g., Curray and Moore (1964); Nielsen and Johannessen (2001)) and can cover extensive areas. Ridges influenced by aeolian processes may produce a relief of 8 m or more (Stapor et al., 1991).

Due to their low relief, beach ridges are difficult to identify in anything but high resolution seismic data. Seismic attribute maps from the lower Brent Group in the North Sea (Jackson et al., 2010) revealed an extensive system of beach ridges preserved at the boundary between the shallow marine Etive Fm. and the overlying Ness Fm. suggesting that these features may be more frequent in the fossil record than previously envisaged. Key morphometric dimension of beach ridge systems used in our study are shown in Table 1.

Table 1: Morphometric data for preserved topographic features (offshore sand ridges, OSS and flooded marginal marine, FMM) capped by the top seal.

Scenario label	OSS	FMM
Amplitude	<20 m	1–10 m
Width	2–4 km	10–300 m
Length	10–60 km	<15 km
Spacing	2–4 km	40–300 m

Buried offshore sand ridges (OSS). Offshore sand ridges are formed on the continental shelf or coastal areas by tidal currents. For our purpose, we have chosen open-shelf ridges as they are prone to have a more regional distribution than estuary mouth and headline associated banks (Dyer and Huntley, 1999). Open shelf ridges are formed in most shallow tidal seas with currents exceeding 0.5 m/s. Present-day examples can be up to 80 km long, up to 13 km wide and tens of meters high. Rising sea levels, changing current conditions or cut-off of sediment supply can cause ridges to become inactive and over time buried beneath marine shale forming a top seal of a series of stratigraphic traps, substantially larger than those created by the buried beach-ridges (FMM).

Reservoir-quality stratigraphic units that have been interpreted as offshore sand ridges include the Tocito sandstone of the San Juan Basin, New Mexico (Riley, 1993; Nummedal and Riley, 1999), the Campanian age Shannon sandstone in Wyoming Suter and Clifton (1999) and the Lower Eocene Vlierzele sands in Belgium (Houthuys and Gullentops, 1988), although the precise genesis of the two first is still somewhat disputed, partly due to limited outcrop exposure of these very large structures. Furthermore, several middle and upper Miocene oil fields on the northwest Java shelf are producing from reservoirs interpreted as shelf sand ridges (Posamentier, 2002) and the reservoir units at the Sleipner field off Norway may also include shelf sand ridges (Nummedal and Suter, 2002). Key morphometric dimensions of the open shelf ridge system used in our study are shown in Table 1. As for FMM their amplitude distribution straddles the margins of seismic resolution.

3.1. Petrophysics

Although both beach ridges and shelf ridges can display a wide range of grain sizes, sorting and internal bedding, including the impact of this was considered beyond the scope of this study. Consequently we kept the

Table 2: Geometric definitions of fault populations for the four faulted reservoir scenarios.

Scenario label	UP1	NP1	UP2	NP2
Displacement	uniform; 100 m	random; 20–150 m	uniform; 100 m	random; 20–150 m
Length	uniform; 4000 m	random; 300–6000 m	uniform; 4000 m	random; 300–6000 m
Strike	uniform; 90°	uniform; 90°	30° and 90°	30° and 90°

petrophysical input simple generic using the same values for all scenarios. In the first and simplest petrophysical scenario we assigned a uniform isotropic permeability of 500 mD and a porosity of 25% to the whole reservoir. In the second petrophysical scenario, the reservoir unit is split in two. The upper part including the ridges in the OSS scenarios was assigned a permeability of 1000 mD and a porosity of 25%. The lower part, representing a more fine-grained substratum across which the ridges migrated when active was assigned a permeability of 400 mD and a porosity of 20%. For comparative purposes, similar petrophysical behaviour was imposed also for the FMM and flat depositional scenarios.

3.2. Structural configurations

Selecting representative realistic tectonic features and fault patterns to include in the models poses some challenges. Although scaling properties of individual faults and fault populations in siliciclastic rocks can be relatively well constrained Torabi and Berg (2011), spatial distribution and orientations of fault populations on our chosen scale tends to be anisotropic and highly case specific. Instead of opting for a specific, (i.e., realistic but unique) spatial configuration we have chosen to use stylised generic patterns with a more isotropic spatial distribution than can be expected at this scale in nature. However, they include features common in most fault systems. This approach also allows an easier identification of links between specific fault parameters and regional plume behaviour.

Four structural configurations were defined in addition to a scenario with no faults; the latter acting as a reference case. Table 2 summarises the parameters used for the four different fault patterns. The dip of the faults is 60 degrees in all cases.

Organising the selected features into a matrix as shown in Figure 1 and

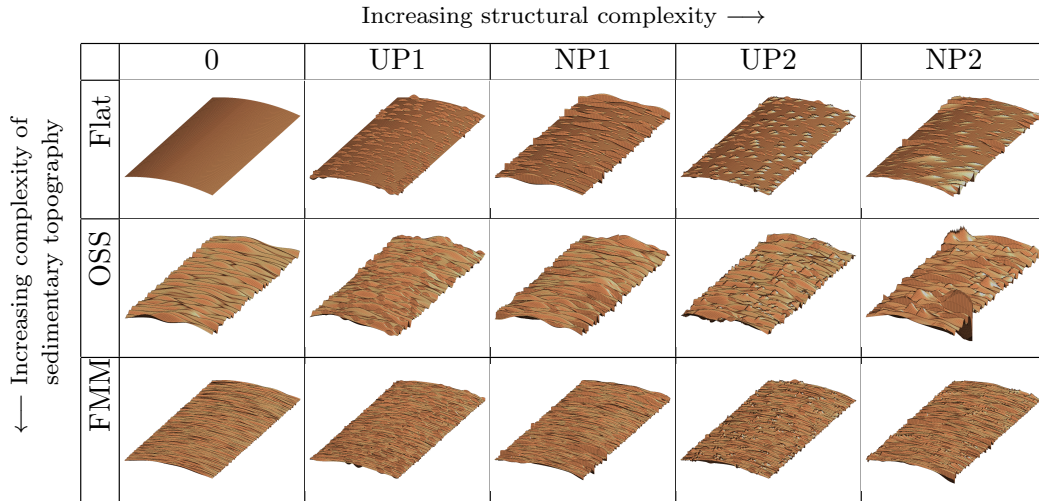


Figure 1: Overview in terms of a heterogeneity matrix for the selected geological features.

running the resulting combinations of structural and sedimentary features allows us to identify the impact of each combination by comparing it to a base case (smooth top reservoir and no faults).

3.3. Stochastic modelling

The geological base-case scenarios described above are modelled by geostatistical methods. In this way, the uncertainty within each model can be explored. A set of top surfaces were generated as follows. First, a base-case surface measuring 30×60 km, with a height difference of 500 meters between the two short ends was created. It has the ideal shape of an inverse half pipe parallel to the longest axis to avoid or minimise leakage over the long edges. The depth of the shallowest point is below 1000 meters to ensure that the CO_2 remains a supercritical phase. The top surfaces of the OSS and FMM models were created by Gaussian random fields and added on top of the base case surface. For both OSS and FMM, a sinusoidal covariance of form $\sin(x)/x$ was used. For OSS, the range along the long axis was 1000 meters, reflecting the width of the lobes, and the range along the short axis was 7000 meters, reflecting the length of the lobes. The standard deviation is 13 meters, reflecting the height of the lobes. For the FMM case, the ranges were 200 meters along the long axis and 700 meters along the short axis, and the standard deviation was 5 meters. This gives us three different stratigraphic models: the base case with flat deposition, offshore sand ridges (OSS), and

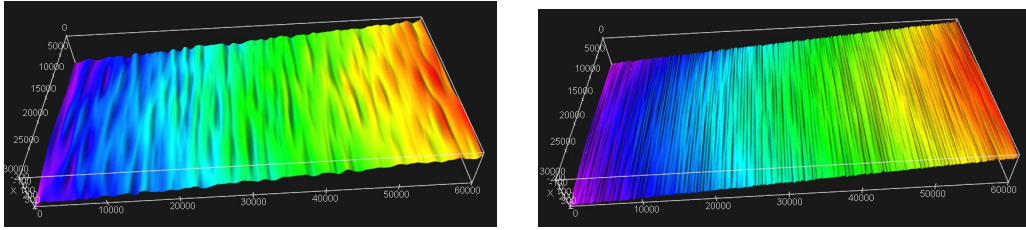


Figure 2: Top surfaces: the left plot shows offshore sand ridges (OSS) and the right plot shows a flooded marginal marine (FMM) deposition.

flooded marginal marine (FMM). These three stratigraphic models were all combined with the four different structural models. The structural models were modelled by the fault modelling tool Havana (Hollund et al., 2002), which is based on a marked point model, using the parameters given in Table 2. Altogether, two hundred faults were generated for each of the models. The combination of stratigraphic and structural models gives us in total fifteen different models; the three stratigraphic models without faults, and each of them combined with four different fault patterns. For each model, except for the base model without faults, 100 realisations were generated and can be downloaded from the IGEMS website (IGEMS, 2011). Examples of simulated top surfaces are shown in Figure 2.

4. Estimation of storage capacity

We consider a simple scenario in which CO_2 is injected from a single well. During injection, the main concern is the pressure build-up during the formation of the CO_2 plume. The top-surface morphology is unlikely to have significant impact on pressure build-up during injection, and herein we will therefore mainly focus on how the morphology affects the degree of structural trapping and the general long-term migration of the CO_2 plume.

Full 3D simulation of several thousand years of plume migration in a $30 \times 60 \text{ km}^2$ reservoir model with a lateral resolution of $100 \times 100 \text{ m}^2$ has a prohibitive computational cost. In this section, we will therefore consider two simplified methods for estimating storage capacity.

4.1. Structural trapping capacity

To estimate the upper theoretical capacity for structural trapping, we will use a geometric analysis to identify the cascade of structural traps associated

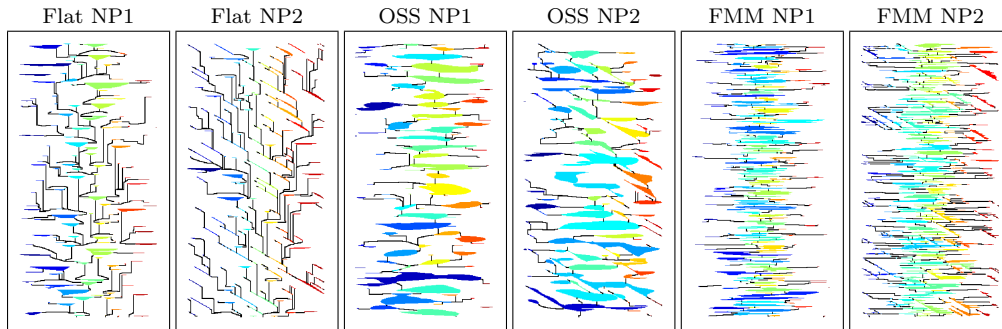


Figure 3: Cascade of traps for specific realisations of six different scenarios.

with a given top-surface morphology. The cascade is defined so that primary traps contain a single local peak, secondary traps contain one saddle-point and more than one peak, tertiary traps contain two saddle-points, etc. The algorithm for identifying the cascade of traps consists of two parts, where the first finds the traps and the second determines the leakage pathways. To find the traps, the following steps are repeated: (1) determine all local maximums as crests of traps; (2) do an argumented depth-first search to find the nearest spill point; (3) replace the trap by the flat surface bounding it from below; and (4) go back to the first step. The four steps are iterated until there are no further local maximums on the updated surface.

Once the cascade of traps has been found, it can be used to bracket the potential for structural trapping, estimate structural trapping for finite injection rates, optimise placement of injection points, etc.

Figure 3 shows six examples of cascades of structural traps. The flat depositional cases only have a few small and scattered traps. The offshore sand ridges have large, but more sparsely scattered traps, whereas the flooded marginal-marine cases have a dense pattern of narrow traps that fill out a larger portion of the formation.

To more systematically study how the top-surface morphology affects capacity estimates for structural trapping, we will consider all the hundred realisations generated for each of the fourteen models described above. For each realisation, we compute the total volume available to residual trapping based upon the cascade of structural traps (that is upslope of the injection point). Table 3 reports the mean volumes for a uniform porosity of 0.25 together with the associated ensemble variation specified in terms of one standard deviation. The structural complexity increases from left to right in

the table, and the complexity of the sedimentary topography increases from top to bottom.

For the flat depositional topography, all structural traps are fault traps. Here, the fault patterns with all faults normal to the flow direction (UP1 and NP1) give larger volumes than the cases that have additional faults with a strike angle of 30° relative to the flow direction (UP2 and NP2). This reduction in volume depends critically on how effective the faults that are not parallel to the trapping structure are at limiting their trapping volume. As expected, we also observe a larger uncertainty in each fault pattern when introducing a random length and displacement.

For the unfaulted cases, all structural traps are fold traps induced by the depositional topography. Here, the case with offshore sand ridges (OSS) has significantly larger storage capacity, mainly because the fold traps have lobes with larger amplitude, width, and length. Compared with the flat depositional cases, we see that the volumes in the fold traps are (almost) one order of magnitude larger than the volumes in the fault traps.

For the cases having a combination of fold and fault traps, faults normal to the flow direction increase the storage capacity, in particular for the flooded marginal marine (FMM) cases. On the other hand, faults having a strike angle of 30° relative to the upslope direction will open some of the fold traps and hence lead to a (slightly) lower structural trapping capacity. Because the OSS scenarios have fewer and larger lobes, the variation between different realisations is larger here than for the FMM cases.

In all the cases considered so far, lobes in the depositional topography are orthogonal to the upslope direction. Rotating the lobes (and the fault strikes) ninety degrees resulted in very small structural trapping capacity as most lobes will be connected to the top of the formation and hence cannot

Table 3: The total volume available for structural trapping for the fifteen different types of top-surface morphologies. The table reports mean volumes in 10^6 m^3 and one standard deviation estimated from one hundred realisations for each scenario assuming a porosity of 0.25.

	unfaulted	UP1	NP1	UP2	NP2
Flat	0 ± 0	96 ± 5	74 ± 23	79 ± 5	50 ± 14
OSS	608 ± 122	648 ± 99	715 ± 120	639 ± 115	629 ± 118
FMM	227 ± 22	278 ± 21	314 ± 38	260 ± 20	259 ± 27

trap significant volumes.

4.2. *Spill-point analysis*

In practise, it will be difficult to utilise all the potential storage capacity of the top surface in a reservoir. To do so, one would have to inject at several places, increasing the operational cost. A more realistic scenario is to use a single injection well, which we will assume is placed (15, 15) km from the south-east corner of the reservoir.

As our first estimate of the potential for structural trapping from a single injection point, we will consider a simple migration model in which fluid is injected at an infinitesimal rate and the buoyant forces dictate flow. In this model, the injected CO₂ will slowly seep upward in the direction of steepest ascent until it encounters the crest of a trap (local maximum point in the top-reservoir morphology), where it will start to accumulate. Once the trap has been filled to its spill point, i.e., to the lowest point that can retain fluids, the CO₂ will leak out and continue to migrate until it is trapped elsewhere or reaches the top of the formation. This type of spill-point calculation is a very fast way of estimating the height of the CO₂ column that may be present within traps that are directly upslope of an injection point and can be used to quickly provide rough estimates of how large part of the available storage volume that can be filled up by injection from a single well for the full model suite.

Figure 4 shows spill point paths for eight different realisations for three of our fifteen scenarios. The figure clearly shows that there are large variations within some of the scenarios. For the flat depositional case, the spill paths mostly follow the ridge in the middle of the reservoir, contacting a different number of traps in the different realisations. The spill paths will deviate more from the middle ridge if we introduce random fault lengths (NP1) and a secondary fault strike (UP2 and NP2). This effect is particularly evident for the FMM NP2 scenario, where we observe that the spill path leaves the reservoir before reaching the top in three of the realisations depicted. Animations showing spill paths of all hundred realisations for each of the fourteen cases can be viewed at the IGEMS website (IGEMS, 2011).

Table 4 reports spill-point estimates of the mean and standard deviation of trapped volumes for the one hundred realisations of each of our fourteen scenarios. As expected, the spill-point volumes are smaller than the total volumes given in Table 3. For the preserved beach ridges (FMM), the spill-point and total volumes are almost the same for the unfaulted case and the

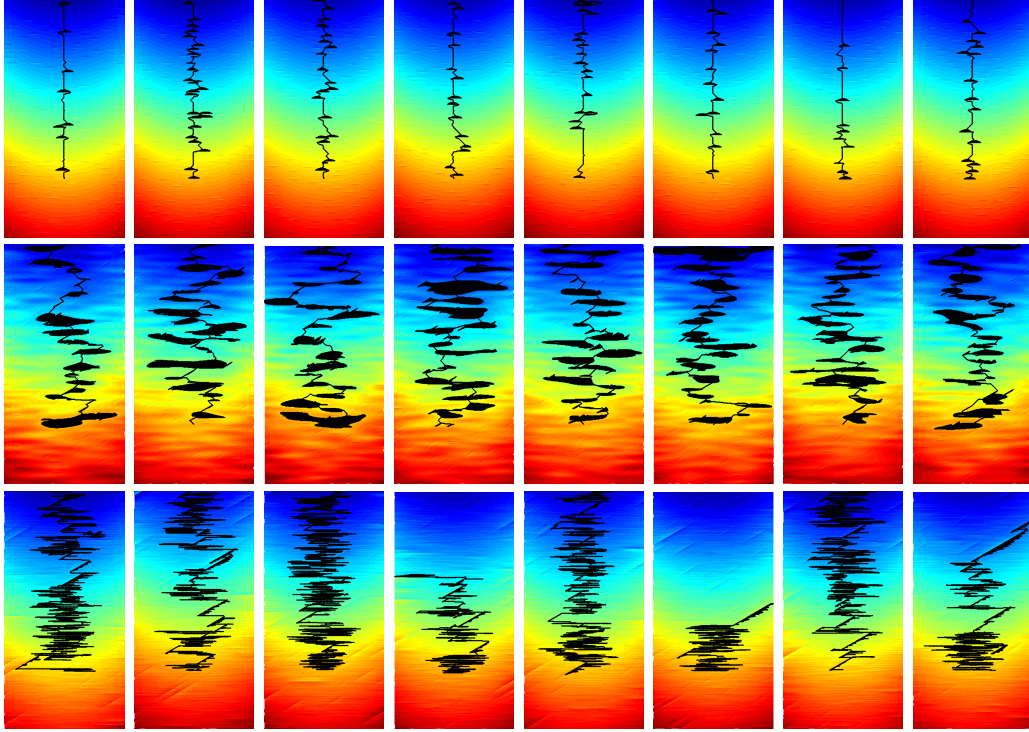


Figure 4: Variations in spill-point paths for different realisations of three different scenarios; from top to bottom: flat UP1, OSS UP2, and FMM NP2.

Table 4: Trapped volumes in units of 10^6 m^3 computed by a spill-point analysis with a single source at coordinates (15, 15) km. Porosity is 0.25.

	unfaulted	UP1	NP1	UP2	NP2
Flat	0 ± 0	20 ± 5	30 ± 19	13 ± 3	15 ± 12
OSS	419 ± 123	431 ± 153	441 ± 180	404 ± 153	379 ± 141
FMM	239 ± 24	268 ± 24	278 ± 94	175 ± 25	184 ± 45

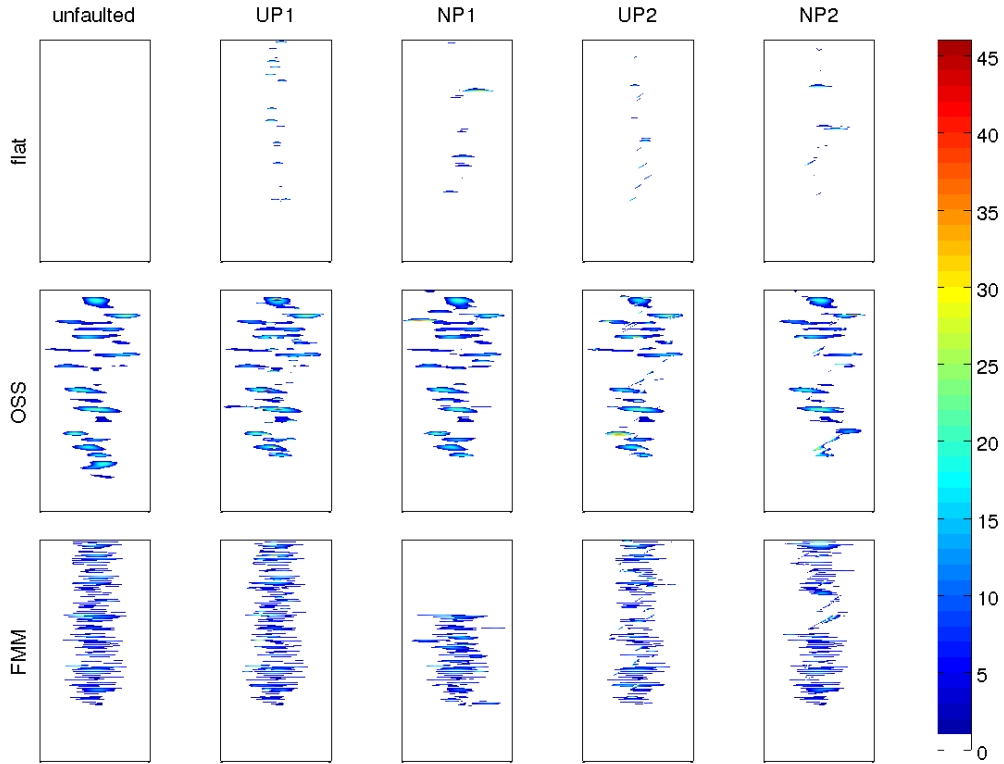


Figure 5: Height in meters inside structural traps computed by a spill-point analysis. The columns show different structural scenarios and the rows different depositional scenarios.

cases without crossing faults (UP1 and NP1). Here, the top-surface lobes are narrow, tightly spaced and relatively long in the transverse direction, which means that the CO_2 will spread out laterally before migrating upslope. This observation is confirmed by the plot in Figure 5, where the height of traps is illustrated for one realisation of each of the fifteen scenarios.

For FMM, we see that the spill path connects with almost all traps in the middle of the formation. However, for the FMM-NP1 case we see that leakage over the edge has prevented the CO_2 from reaching the top, as was previously observed for the FMM-NP2 case in Figure 4. The mean trapped volume will therefore be much smaller than the total available volume in this case. Leakage also explains why the variation in Table 4 has increased significantly compared to Table 3 for some of the OSS and FMM scenarios. If cases with leakage at edges are disregarded, the variation in volumes becomes

Table 5: Volumes in units 10^6 m^3 from spill-point calculations with varying placement of the injection point.

	unfaulted	UP1	NP1	UP2	NP2
Flat	0 ± 0	21 ± 2	32 ± 3	11 ± 2	19 ± 11
OSS	311 ± 94	366 ± 121	340 ± 106	317 ± 48	250 ± 75
FMM	272 ± 21	276 ± 20	182 ± 24	208 ± 17	196 ± 22

more similar to the values given in Table 3.

For the cases with crossing faults, UP2 and NP2, we see in Figure 5 that the upslope migration is enhanced, and the lateral filling is reduced. The spill-point analysis predicts that approximately 67 % and 71% of the available volume will be filled. For offshore sand ridges, the spill-point analysis predicts a filling degree of 60–69%. The lobes are much larger in this case, and spill paths may miss large traps on their way to the top. For the flat depositional cases, the spill path will only reach a few of the available fault traps, and the analysis predicts that only 16–40% of the total available volume is filled with CO_2 with the chosen injection point. For cases with only fault traps, more injection points are needed to fill more of the available storage volume.

We also investigated the dependency on the location of the injection point. This was conducted by selecting one realisation of each scenario, and considering fifteen different injection points placed on a regular mesh (x, y) with nodes at $x = 5, 10, \dots, 25$ km, and $y = 10, 15, 20$ km. The trapped volumes calculated by the spill-point approach is shown in Table 5. We observe that the variation in volumes is largest in the OSS case like we also observed above. On the other hand, the variation due to changing the injection point is smaller than the variation caused by the stochastic model. The choice of injection point location does therefore not seem to be critical for the degree of filling.

5. Flow simulation

The migration of CO_2 is a true multiscale problem with a large disparity in spatial and temporal scales. CO_2 is mobile and will typically migrate over large distances before becoming fully trapped. During migration, however, the flow is usually confined to thin layers underneath the caprock and resolving the migration accurately may require a very fine vertical resolution

in 3D simulations.

Using a vertical equilibrium (VE) assumption (Nordbotten and Celia, 2012), the flow of a thin CO₂ plume can be approximated in terms of its thickness to obtain a 2D simulation model. Although this approach reduces the dimension of the model, important information of the heterogeneities in the underlying 3D medium is preserved. In fact, the errors resulting from the VE assumption will in many cases be significantly smaller than the errors introduced by the overly coarse resolution needed to make the 3D simulation model computationally tractable. In addition, integrating the flow equations vertically improves the time constants of the model and typically leads to a looser dynamical coupling, e.g., between flow and transport. Vertical equilibrium simulations will therefore in many cases be an attractive method to increase (lateral) resolution while saving computational cost, in particular for scenarios similar to those considered herein.

As above, our injection scenario consists of a single well positioned at (15,15) km, which will inject at a constant rate of ten million cubic meters per year for 50 years. In total, we will follow the formation of a CO₂ plume and its subsequent upslope migration for a period of 5000 years. Fluid properties will generally depend on pressure and thus height along the formation. To simplify the flow simulations, we neglect the pressure dependence and assume all fluids to be incompressible and be described by the following fluid parameters: CO₂ is assumed to be a supercritical fluid with viscosity of 0.057 cP, constant density of 686 kg/m³, and a quadratic relative permeability with residual saturation of 0.2 and endpoint scaling factor of 0.2142. For water, we assume a viscosity of 0.31 cP, density of 975 kg/m³, residual saturation of 0.1, and endpoint scaling of 0.85. During injection we impose hydrostatic boundary conditions, whereas no-flow boundary conditions are assumed during the post-injection period.

5.1. Estimates of trapping

We start by considering one realisation of each of the fifteen scenarios with the uniform petrophysical model. Figure 6 compares structural trapping estimated by flow simulation with similar estimates calculated by the spill-point approach, whereas Figure 7 shows the height of plumes of free CO₂ for all the fifteen scenarios. By comparing with Figures 5 and 7, we see that the VE simulation predicts that the CO₂ plume will spread laterally and therefore potentially contact more traps on its upslope migration than what is predicted by the spill-point analysis. This explains why the VE

simulation predicts larger structural trapped volumes for the flat depositional scenarios. For the OSS and FMM scenarios, the VE simulation predicts that the plume has not reached the top of the structure after 5000 years in most of realisations. The spill-point calculation, on the other hand, continues to fill traps until some CO₂ reaches the top of the formation, and hence overestimates the volumes that are structurally trapped after 5000 years.

With flow simulation, we can also find free and residually trapped volumes. The free volume is defined as the volume that is not residually trapped, and includes volumes confined in fold and fault traps. Figure 8 gives the free and residually trapped volumes computed by flow simulation. We observe that the residual trapping is largest for the flat depositional cases, for which the plume has reached the top of the structure within 5000 years. In this case, there is almost no relief in the top-surface morphology that will retard the plume migration and hence the plume will sweep a large volume within the migration period. For the OSS and FMM scenarios, the plume is retarded by the lobes in the top surface, and residual trapping is reduced compared with the surface without reliefs. Eventually, however, the residual trapping will increase also for these scenarios.

The most striking observation that can be made from Figures 6 to 8 is that structure has a limited influence on the free and residual volumes compared with the sedimentary scenarios OSS and FMM. In practise, this means that top-surface morphology caused by faulting has less effect than the morphology caused by sedimentary architectures. This is an interesting observation given that modellers tend to put a lot of effort into describing faults and ignore sedimentary effects on the top-surface morphology. (On the other hand, our observation may be biased by the fact that we have used simple fault model in which all faults are assumed to be sealing.)

5.2. Effect of high-permeable top

Both beach rides and shelf ridges will often have a higher grain size towards the top, which is reflected in a simple way by our second petrophysical model that has a high-permeable top layer.

Figures 9 and 10 report differences in movable and structurally trapped CO₂ volumes, respectively, predicted by the two models. A high-permeable top leads to increased structural trapping in all cases except for OSS-NP2, but has different effects on the movable volume for the three sedimentary scenarios. Figures 11 and 12 show that for the FMM and the flat depositional scenarios, the plume will move faster to the top, thereby increasing the

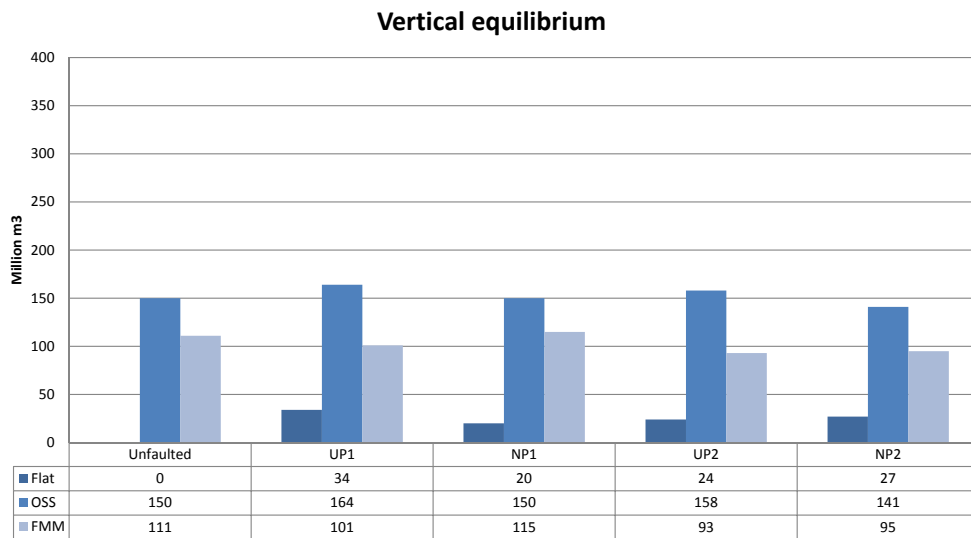
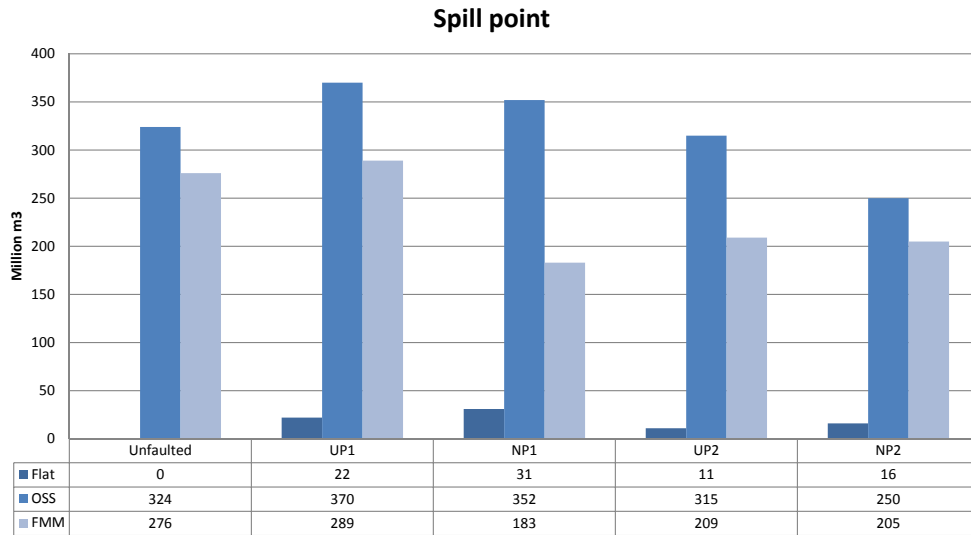


Figure 6: Comparison of structurally trapped volumes in units of million cubic meters computed by spill-point analysis and VE simulation.

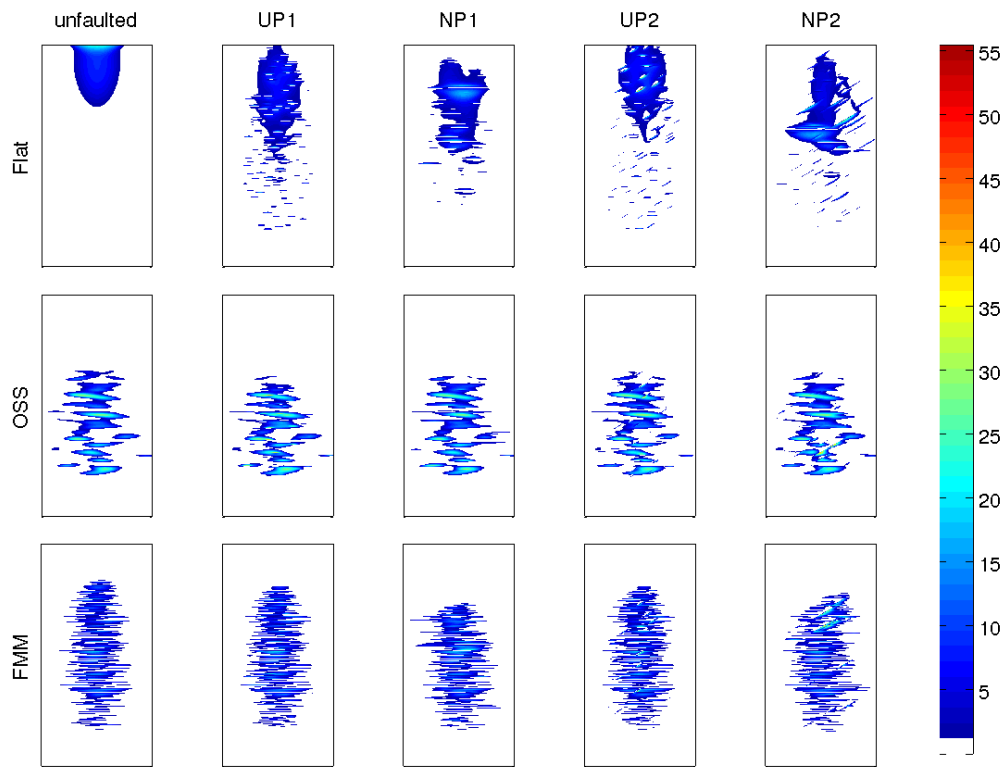


Figure 7: Height in meters for the plumes of free CO₂ after 5000 years. The columns show different structural scenarios and the rows different depositional scenarios.

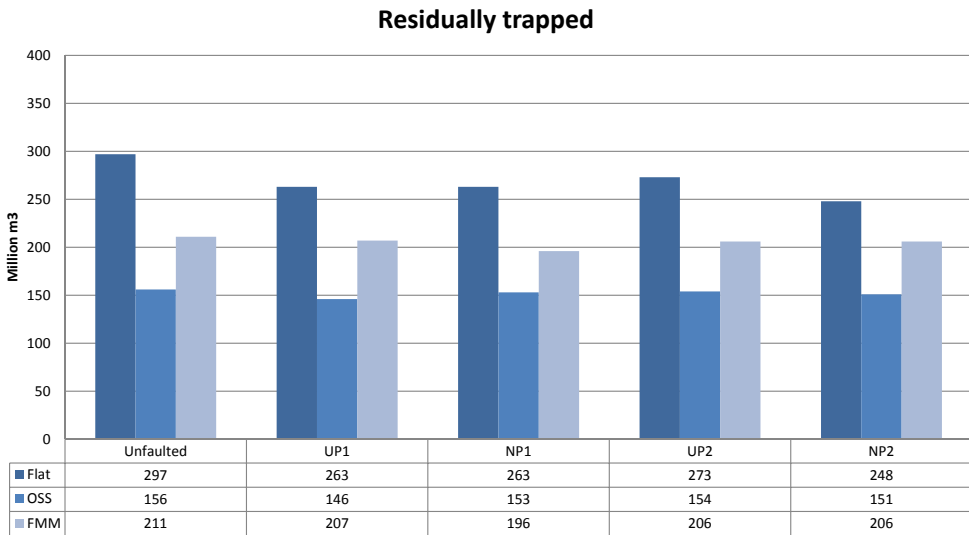
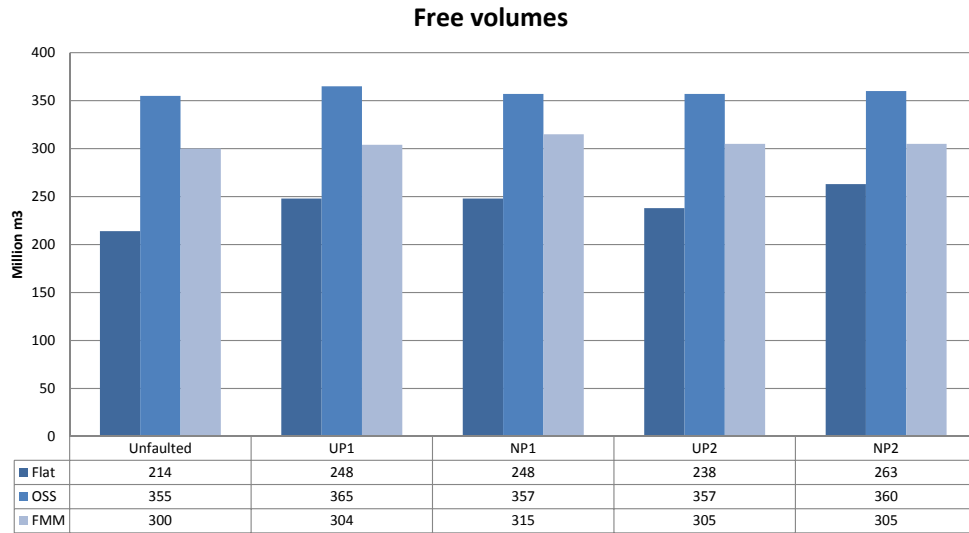
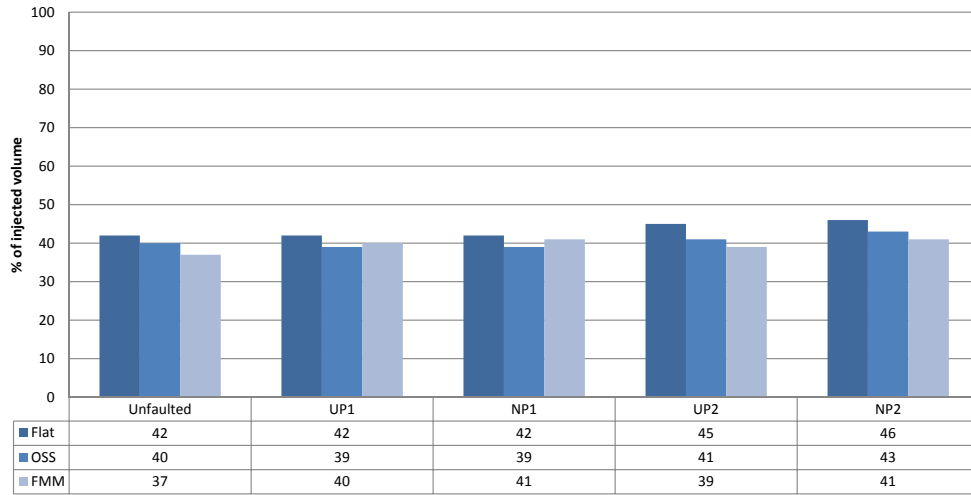


Figure 8: Free and residually trapped volumes in units of million cubic meters computed by a VE simulation.

Uniform Permeability; free volumes



High Permeability top; free volumes

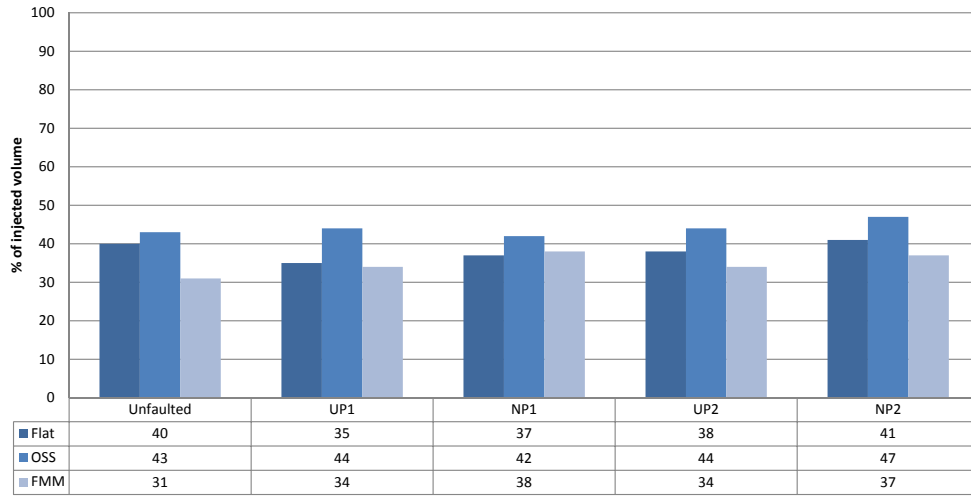
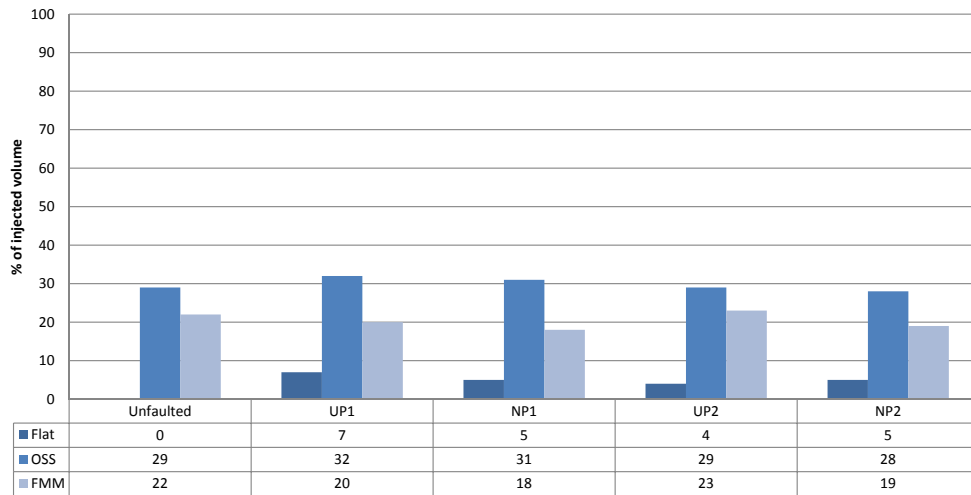


Figure 9: Volumetric fraction of the injected CO₂ that is movable (free) after 5000 years for one realisation of each scenario and two permeability models: uniform and high-permeable top.

Uniform Permeability; residually trapped volumes



High Permeability top; residually trapped

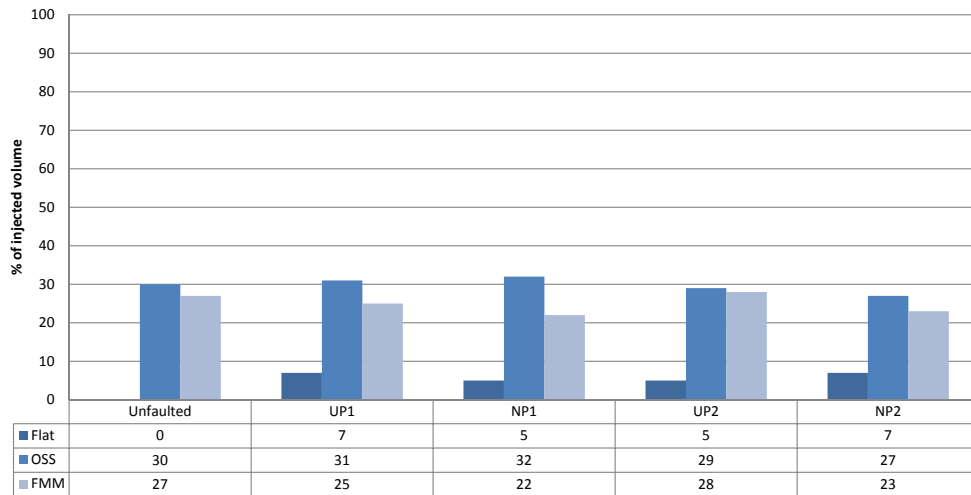


Figure 10: Volumetric fraction of the injected CO₂ that is residually trapped after 5000 years for one realisation of each scenario and two permeability models: uniform and high-permeable top.

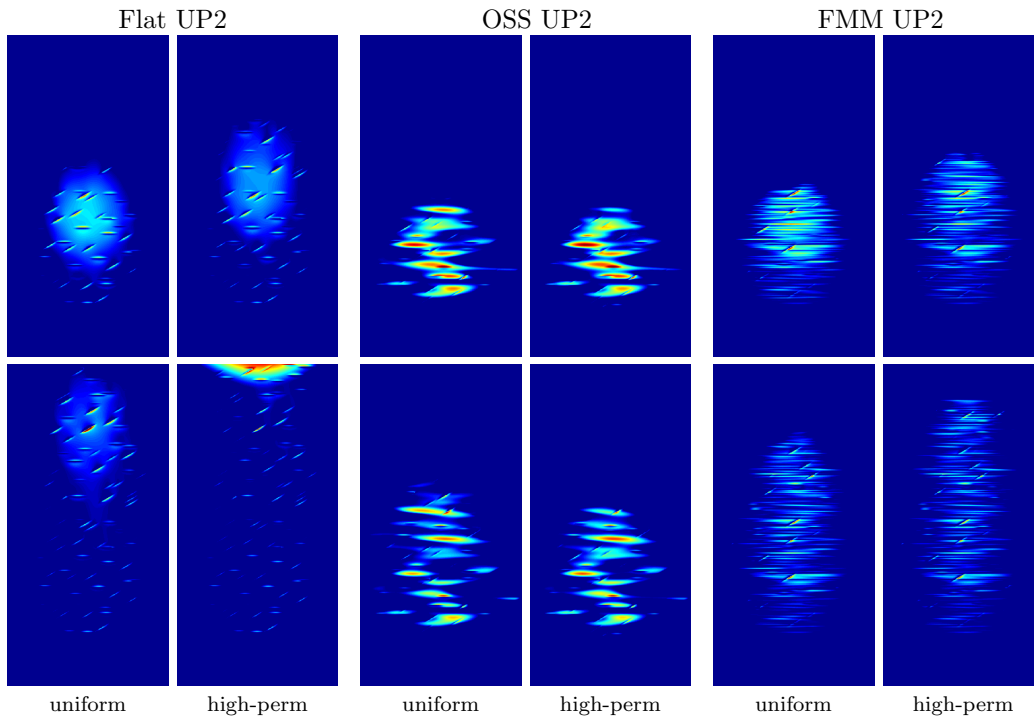


Figure 11: Height of the CO₂ plume after 1425 years (top) and 4525 years (bottom) for structural model UP2, the three different sedimentary scenarios, and the two petrophysical models.

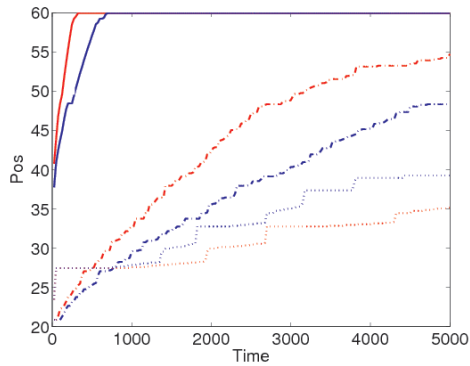


Figure 12: Maximum upslope position (in kilometres) of the CO₂ plume as a function of time (in years) for the three sedimentary scenarios: flat (solid line), OSS (dotted), and FMM (dash-dot). Blue colour denotes uniform permeability and red denotes high-permeable top layer.

residual trapping and decreasing the movable volume. For the OSS scenarios, on the other hand, a high-permeable top will *retard* the plume migration and thus increase the volume fraction that is movable after 5000 years. Here, the height of the lobes in the top surface is so large that many spill points will be located within the low-permeable part of the reservoir.

6. Coarsening the top surface

In the simulations described above, we have used a relatively simple flow model that only accounts for incompressible two-phase effects. For such a simple flow model, there are several methods available that enable forward simulations to be conducted with high efficiency. Herein, we used vertical integration of the flow equations that reduced the computational cost of the flow simulation and enabled us to run a single forward simulation at the full model resolution within hours on a powerful workstation. However, even with a sixteen-core shared-memory computer at our disposal, we still found that running fully resolved flow simulations for the whole ensemble of $2 \times 14 \times 100$ model realisations was computationally intractable within a few days. One may, of course, argue that the problem would be computationally tractable if we had chosen a more powerful computer or extended our time frame. On the other hand, the computational cost associated with each forward simulation will increase dramatically once one starts to add more physical effects into the flow model. In our opinion, some degree of upscaling of our geological representation is therefore inevitable to allow us to conduct a full Monte Carlo type uncertainty analysis. To this end, we will consider a simple upscaling in which the grid is coarsened a factor two or a factor four in each lateral direction so that the new top surface can be obtained by a straightforward resampling (interpolation).

In the remains of this section, we will investigate to what extent the grid models can be coarsened without losing relevant detail. First of all, coarsening the grid may potentially change the top surface and thereby the volumes available for structural trapping. Figure 13 shows how this will affect our estimates for the volume available to structural trapping. The effect is most pronounced for the FMM cases, which have the most detailed geometry in the form of small and densely populated lobes that are flattened when resampled on a coarser grid. Hence, the fine-scale details are not conserved during coarsening and structurally trapped volumes become too small. The OSS sedimentary cases, on the other hand, have significantly larger lobes and

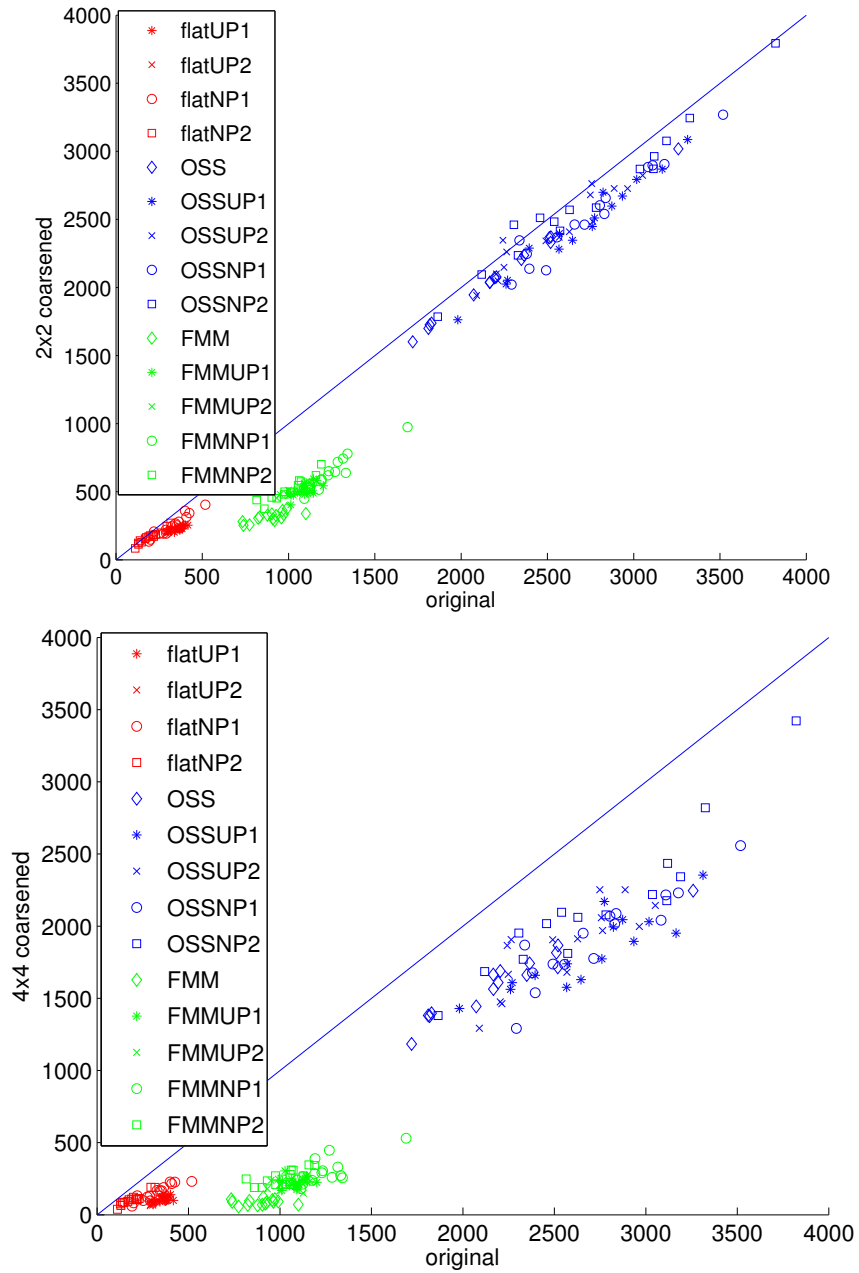


Figure 13: Scatter plot of total volume available in structural traps for coarsened surfaces versus the same volume from the original grid for fifteen realisations of each of the fourteen scenarios. To the left, a factor two is used in the coarsening, to the right the coarsening factor is four.

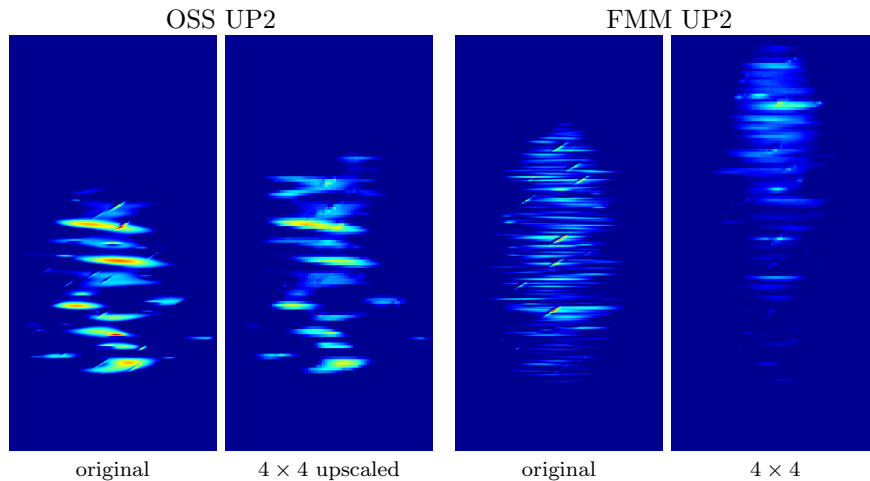


Figure 14: Height of the CO₂ plume after 1425 years (top) and 4525 years (bottom) for structural model UP2, the three different sedimentary scenarios, and the two petrophysical models.

here the volume of the traps is reasonably preserved for the 2×2 coarsening but not for the 4×4 coarsening. The flat depositional cases are somewhere in between.

There are, of course, better ways to upscale the top surfaces. A first alternative is to use a non-Cartesian and possibly unstructured grid that would better preserve the geometry of the top surface and thereby the volume of the structural traps. A second alternative is to upscale the relative permeability and capillary pressure curves, using a techniques from flow-based upscaling that would naturally lead to tensorial relative permeabilities. Work has been done in this direction, but no such calculations have been performed on the IGEMS data set.

We have seen above how large reliefs in the top-surface morphology retards the upslope migration of the CO₂ plume. As coarsening the surface will remove detail, we must expect that it also will diminish the retardation effect. This is confirmed in Figure 14, which shows snapshots of the plume migration for two different scenarios. In both cases, we see that the 4×4 coarsened surfaces underestimate the structurally trapped volumes and the retardation caused the top-surface morphology, in particular for the FMM case. How fast the plume migrates upslope will affect both the structural trapping and the fraction of the volume that is movable at any time. Figures 15 and 16 confirm that the FMM case is most influenced by the upscaling and that coarsening

the surface here will produce a significant, and possibly unacceptable, bias in the estimates. For the OSS and flat depositional scenarios, more reliable estimates can be obtained also from the upscaled models.

For completeness, we also show how coarsening the top surface affects the distribution functions that can be derived from the one hundred realisations. Figure 17 shows histograms for structural scenario NP2 with different upscaling factors for all three sedimentary scenarios. Here, we clearly observe that whereas the distribution functions for the OSS and flat depositional scenarios are only slightly perturbed, the FMM distribution shifts significantly along the axis with increasing degree of coarsening.

7. Discussion

In the previous sections we have shown both simplified geometrical analysis of structural trapping (spill point and cascades of traps) as well as estimates based upon more comprehensive flow simulations. Fast estimation of fluid responses is essential to use a Monte Carlo type approach to study the influence of geological uncertainty on plume migration and fluid trapping. Hence, a key question is: how reliable estimates can we get from the simplified models?

Figure 18 shows the correlation between the theoretical capacity for structural trapping estimated from the cascade of traps and the structurally trapped volumes estimated by fluid simulation. For the FMM and flat depositional scenarios, which both have small-scale reliefs in their morphology, the two estimates correlate well. The OSS scenarios, on the other hand, show much larger variation because of the larger lobes and although a geometrical analysis may give indicative numbers of actual trapping, this type of estimate will generally be less reliable.

Figure 19 shows a similar correlation plot for residual trapping versus volumes available. The figure indicates a negative correlation between the two, which is somewhat misleading. Instead, the figure shows the correlation between structural volume and how much the plume migration is retarded; see the discussion above. After 5000 years, the plume has reached the top and all possible residual trapping has taken place for the flat depositional scenarios. For the OSS and FMM scenarios, the plume has not yet reached the top and further residual trapping is likely to take place at a later time.

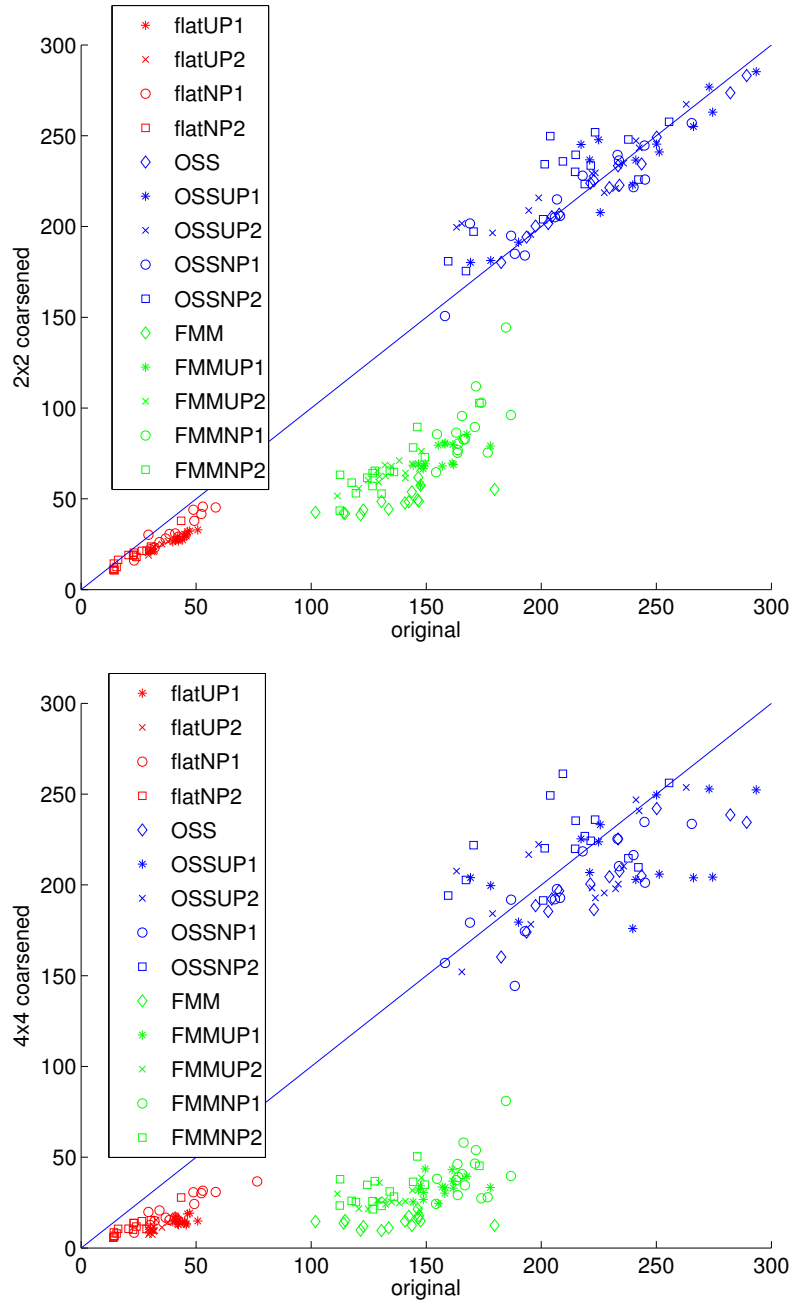


Figure 15: Scatter plot of structurally trapped volumes estimated from coarsened surfaces versus the same volumes estimated from the original surface.

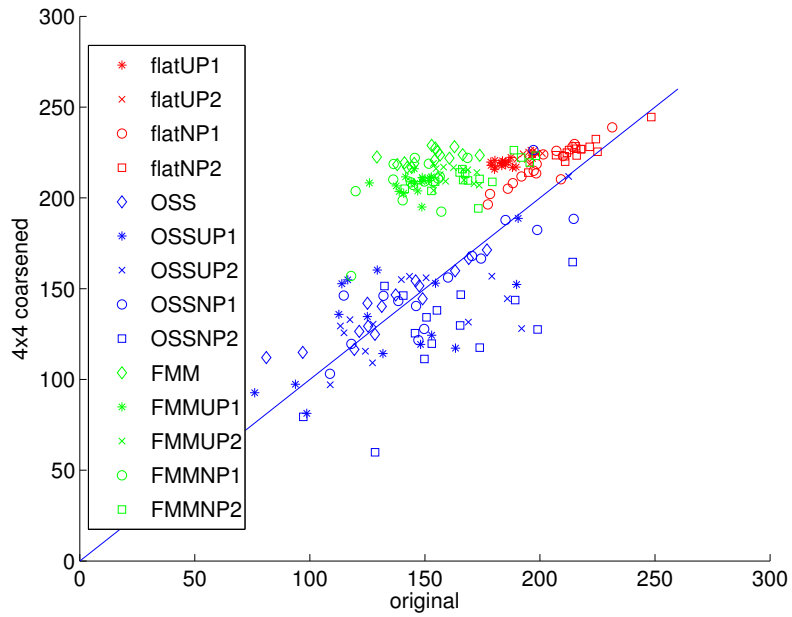
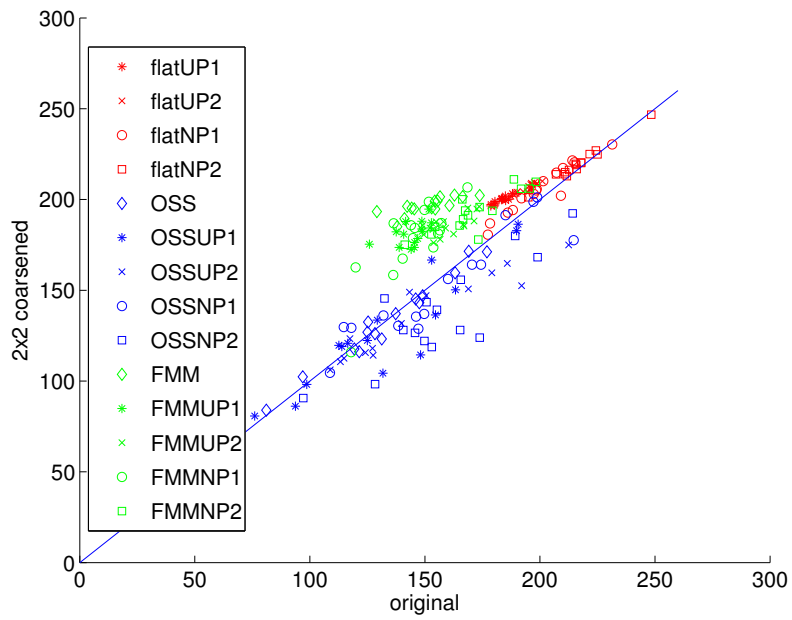


Figure 16: Scatter plot of movable volume estimated from coarsened surfaces versus the same volumes estimated from the original surface.

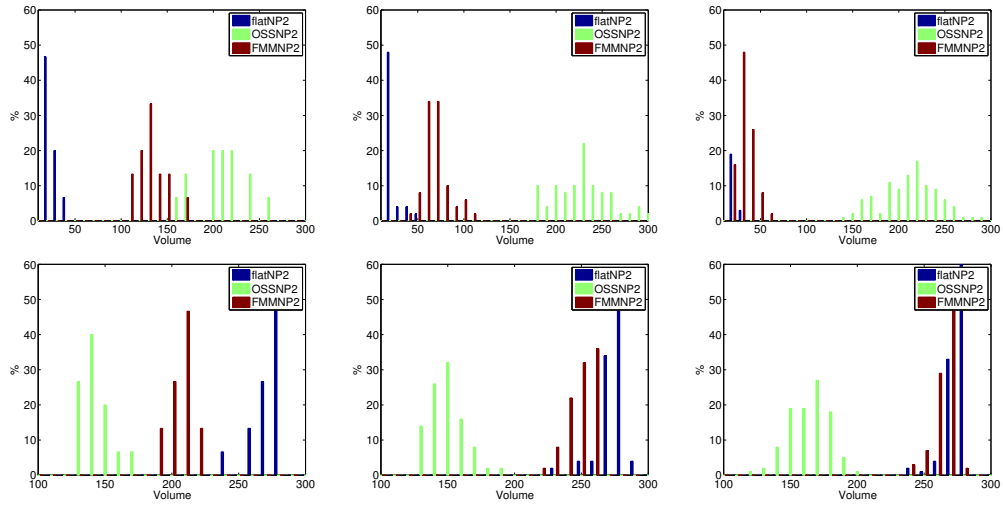


Figure 17: Histogram of the distribution of structurally trapped volumes (upper row) and residually trapped volumes (lower row) for three different scenarios.

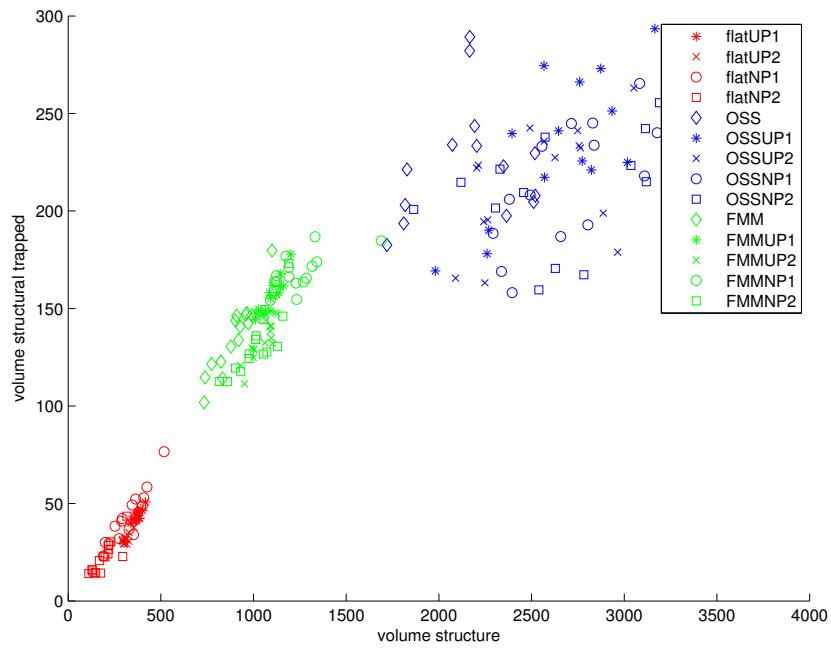


Figure 18: Correlation between the volume available in structural traps and the structurally trapped volumes estimated by a flow simulation.

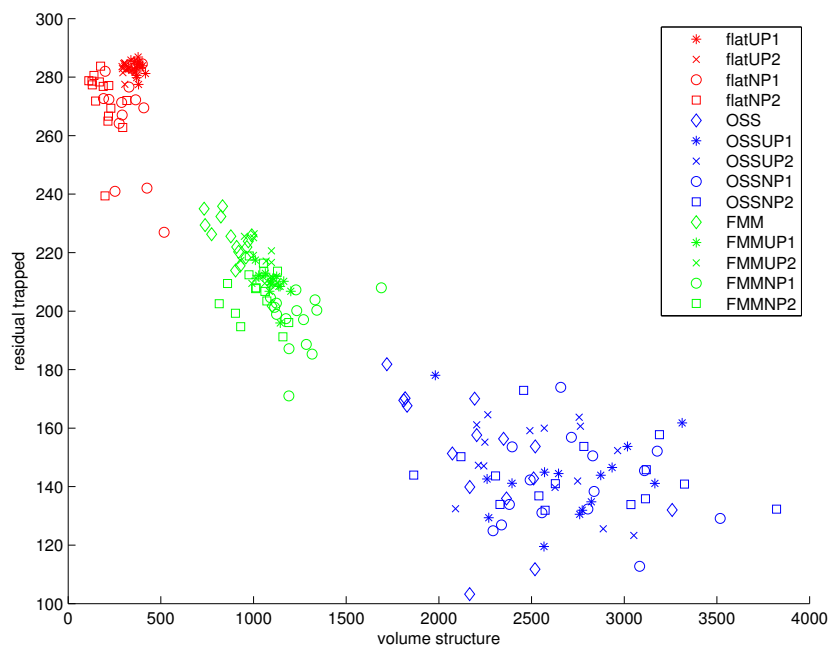


Figure 19: Correlation between the volume available in structural traps and the residually trapped volumes estimated by a flow simulation.

8. Conclusion

Trapping of CO₂ is significantly affected by top-surface morphology, which contributes both to structural trapping and retardation of the plume migration. As a result, the statistics of the top-surface morphology has a strong influence on the statistics of the trapped fluid. However, the spread of the plume is only inhibited if the height of the plume is of the same scale as the amplitude of the relief. A modest relief may therefore retard the migration for low injection rates, but have negligible effect for high injection rates that create a thick plume.

For the specific parameters considered herein, structural and residual trapping are equally important. More surprising, we observe that faulting has less influence on the free and residual volumes than the top-surface morphology induced by sedimentary architecture, which is often neglected in geological modelling. Our observation may be an effect of overly simplified model choices, but should nevertheless be more thoroughly investigated because of its potential implications of how large-scale aquifers should be modelled.

The interplay between structural and residual trapping is generally non-trivial. Still, our analysis shows that the potential for structural trapping can be efficiently estimated for large model ensembles using simplified modelling: Cascades of structural traps are effectively identified by a simple geometrical analysis and can be used to bound the structural trapping capacity. Likewise, rough estimates for actual trapping from specific injection points can be efficiently calculated using a spill-point analysis. Residual trapping, on the other hand, appears to be less correlated with simple volume estimates and must generally be resolved by detailed flow simulations. To this end, models based upon vertical integration have proved very useful because of significantly reduced computational cost and improved vertical resolution compared with traditional 3D modelling.

The need for further upscaling, and the effect that such an upscaling has on flow predictions, will depend highly on the sedimentary and structural scenarios. Our scenarios with buried offshore sand ridges (OSS) have large lobes and are not strongly affected by (modest) coarsening of the top surface. The flooded marginal-marine (FMM) scenarios, on the other hand, consist of dense patterns of small-scale structures that are quite sensitive to grid resolution and cannot be coarsened geometrically in a straightforward way without losing essential detail. One alternative is to use a more elaborate

flow-based upscaling, but this may lead to complicated models with tensorial relative permeabilities.

Altogether, our analysis demonstrates that uncertainty in morphology effects at a small scale may have a significant impact on estimates of structural and residual trapping. A future research direction would therefore be to develop a more truly multiscale framework that can properly account for small-scale effect when simulating large-scale CO₂ plume migration.

9. Acknowledgements

This work was supported by the Norwegian Research Council through grant no. 200026 from the CLIMIT programme.

References

- Ashraf, M., Lie, K.-A., Nilsen, H. M., Skorstad, A., 2010. Impact of geological heterogeneity on early-stage CO₂ plume migration: sensitivity study. In: Proceedings of the 12th European Conference on the Mathematics of Oil Recovery (ECMOR XII), Oxford, UK, 6–9 September 2010. EAGE.
- Celia, M. A., Nordbotten, J. M., Bachu, S., Kavetski, D., Gasda, S., 2010. Summary of princeton workshop on geological storage of CO₂. Princeton-bergen series on carbon storage, Princeton University, uri: <http://arks.princeton.edu/ark:/88435/dsp01jw827b657>.
- Chadwick, A., Williams, G., Delepine, N., Clochard, V., Labat, K., Sturton, S., Buddensiek, M., Dillen, M., Nickel, M., Lima, A., Arts, R., Neele, F., Rossi, G., 2010. Quantitative analysis of time-lapse seismic monitoring data at the Sleipner CO₂ storage operation. *The Leading Edge*, 170–177.
- Chadwick, R. A., Noy, D. J., 2010. History-matching flow simulations and time-lapse seismic data from the Sleipner CO₂ plume. In: *Petroleum Geology: From Mature Basins to New Frontiers Proceedings of the 7th Petroleum Geology Conference*. Vol. 7 of Petroleum Geology Conference series. Geological Society, London, pp. 1171–1182.
- Class, H., Ebigbo, A., Helmig, R., Dahle, H. K., Nordbotten, J. M., Celia, M. A., Audigane, P., Darcis, M., Ennis-King, J., Fan, Y., Flemisch, B., Gasda, S. E., Jin, M., Krug, S., Labregere, D., Beni, A. N., Pawar, R. J.,

- Sbai, A., Thomas, S. G., Trenty, L., Wei, L., 2009. A benchmark study on problems related to CO₂ storage in geologic formations. *Comput. Geosci.* 13 (4), 409–434.
- Curray, J. R., Moore, D. G., 1964. Holocene regressive littoral sand, Costa de Nayarit, Mexico. In: Van Straaten, L. M. J. U. (Ed.), *Deltaic and Shallow Marine Deposits*. Elsevier, pp. 76–82.
- Dyer, K. R., Huntley, D. A., 1999. The origin, classification and modelling of sand banks and ridges. *Continental Shelf Research* 19, 1285–1330.
- Eiken, O., Ringrose, P., Hermanrud, C., Nazarian, B., Torp, T., Hier, L., 2011. Lessons learned from 14 years of ccs operations: Sleipner, In Salah and Snøhvit. *Energy Procedia* 4, 5541–5548.
- Hollund, K., Mostad, P., Nielsen, B. F., Holden, L., Gjerde, J., Contursi, M. G., McCann, A. J., Townsend, C., Sverdrup, E., 2002. Havana — a fault modeling tool. In: Koestler, A. G., Hunsdale, R. (Eds.), *Hydrocarbon Seal Quantification*. Norwegian Petroleum Society Conference, 16–18 October 2002, Stavanger, Norway. Vol. 11 of NPF Special Publication. Elsevier.
- Houthuys, R., Gullentops, F., 1988. The Vlierzele Sands (Eocene, Belgium): a tidal ridge system. In: *Tide-influenced sedimentary environments and facies*. D. Reidel Publishing Co., Dordrecht, pp. 139–152.
- IGEMS, 2011. Impact of realistic geologic models on simulation of co₂ storage (igems). <http://igems.nr.no>.
- Jackson, C. A.-L., Grünhagen, H., Howell, J. A., Larsen, A. L., Andersson, A., Boen, F., Groth, A., 2010. 3D seismic imaging of lower delta-plain beach ridges: lower Brent Group, northern North Sea. *Journal of the Geological Society of London* 167, 1225–1236.
- Manzocchi, T., et al., 2008. Sensitivity of the impact of geological uncertainty on production from faulted and unfaulted shallow-marine oil reservoirs: objectives and methods. *Petrol. Geosci.* 14 (1), 3–15.
- Nielsen, L. H., Johannessen, P. N., 2001. Accretionary, forced regressive shoreface sands of the Holocene-recent Skagen Odde spit complex, Denmark – a possible outcrop analogue to fault-attached shoreface sandstone

- reservoirs. In: Martinsen, O. J., Dreyer, T. (Eds.), *Sedimentary Environments Offshore Norway Palaeozoic to Recent*. Vol. 10 of NPF special publication. Norsk petroleumforening, Elsevier, pp. 457–472.
- Nordbotten, J. M., Celia, M. A., 2012. *Geological Storage of CO₂: Modeling Approaches for Large-Scale Simulation*. John Wiley & Sons.
- Nummedal, D., Riley, G. W., 1999. The origin of the Tocito Sandstone and its sequence stratigraphic lessons. In: *Isolated Shallow Marine Sand Bodies: Sequence Stratigraphic Analysis and Sedimentologic Interpretation*. Vol. 64 of SEPM Special Publication. Bergman, K. M. and Snedden, J. W., pp. 227–254.
- Nummedal, D., Suter, J., 2002. Continental shelf sand ridges; genesis, stratigraphy and petroleum significance. In: *22nd Annual Gulf Coast Section SEPM Foundation Bob F. Perkins Research Conference Proceedings*. pp. 503–518.
- Otvos, E. G., 2000. Beach ridges definition and significance. *Geomorphology* 32, 83–108.
- Posamentier, H. W., 2002. Ancient shelf ridges—a potentially significant component of the transgressive systems tract: case study from offshore north-west Java. *AAPG Bullentine* 86, 75–106.
- Pruess, K., Garca, J., Kavscek, T., Oldenburg, C., Rutqvist, J., Steefel, C., Xu, T., 2004. Code intercomparison builds confidence in numerical simulation models for geologic disposal of CO₂. *Energy* 29 (9–10), 1431–1444.
- Riley, G. W., 1993. *Origin of a coarse-grained shallow marine sandstone complex: the Coniacian Tocito Sandstone, northwestern New Mexico*. Ph.D. thesis, Louisiana State University.
- Stapor, F. W. J., Matthews, T. D., Lindfors-Kearns, F. E., 1991. Barrier-island progradation and Holocene sea-level history in southwest Florida. *Journal of Coastal Research* 7, 815–838.
- Suter, J. R., Clifton, H. E., 1999. The Shannon Sandstone and isolated linear sand bodies: interpretations and realizations. In: *Isolated Shallow Marine Sand Bodies: Sequence Stratigraphic Analysis and Sedimentologic*

Interpretation. Vol. 64 of SEPM Special Publication. Bergman, K. M. and Snedden, J. W., pp. 321–356.

Torabi, A., Berg, S. S., 2011. Scaling of fault attributes: A review. *Marine and Petroleum Geology* 28, 1440–1460.